

Investigation of elemental mercury removal from the coal-fired boiler flue gas over MIL101-Cr

Lu Dong^{1,2}, Yaji Huang^{1}, Lingqin Liu¹, Changqi Liu¹, Ligang Xu¹, Jianrui Zha¹, Hao Chen¹,*

Hao Liu^{2}*

¹Key Laboratory of Energy Thermal Conversion and Control of Ministry of Education, School of Energy and Environment, Southeast University, Nanjing 210096, China

²Faculty of Engineering, University of Nottingham, University Park, Nottingham, NG7 2RD, England, UK

Corresponding authors

*Yaji Huang, heyyj@seu.edu.cn

*Hao Liu, liu.hao@nottingham.ac.uk

Abstract

In this work, the MIL101-Cr sorbent with a large BET surface area was prepared and used to remove Hg⁰ from the simulated coal-fired boiler flue gas. The chemical and physical properties of the prepared sorbent were characterized by X-ray diffraction (XRD), Brunauer-Emmett-Teller (BET) and X-ray photoelectron spectroscopy (XPS). A range of experiments was conducted in a fixed-bed reactor to investigate the effects of reaction temperature, Hg⁰ inlet concentration, gas hourly space velocity

(GHSV) and flue gas composition on the Hg^0 removal for the prepared sorbent. The mechanisms and kinetics of the Hg^0 adsorption were also studied. The results showed that the MIL101-Cr sorbent achieved the Hg^0 removal efficiency of more than 85% for 4 h at 200 °C under the condition of a relatively high Hg^0 inlet concentration ($203 \mu\text{g}/\text{m}^3$) and GHSV ($8 \times 10^5 \text{ h}^{-1}$). The O_2 in the flue gas was found to be beneficial to Hg^0 removal. The NO in the flue gas favoured Hg^0 removal both in the presence and absence of O_2 . The SO_2 in the flue gas notably inhibited Hg^0 adsorption in the absence of O_2 , whereas a low concentration of SO_2 slightly inhibited Hg^0 removal in the presence of O_2 . However, high concentrations of SO_2 in the flue gas still significantly weakened Hg^0 removal ability even in the presence of O_2 due to the competitive adsorption of SO_2 with Hg^0 on the sorbent and the sulfation of the sorbent. A simultaneous presence of O_2 and NO in the flue gas could overcome the adverse impact of SO_2 on Hg^0 adsorption. The H_2O has little influence on Hg^0 removal due to the competitive adsorption. The XPS analysis indicated that the surface Cr^{3+} , oxygen species and C=O group in MIL101-Cr acted as the active adsorption/oxidation sites for Hg^0 . The Hg^0 removal by MIL101-Cr belonged to chemisorption and could be described by the pseudo-second-order model. The equilibrium adsorption capacity calculated for the sorbent amounted to $25656 \mu\text{g}/\text{g}$ at 200 °C, which indicated that MIL101-Cr could be used as a promising sorbent to remove Hg^0 from the coal-fired boiler flue gas.

Keywords: MIL101-Cr; Elemental Mercury; Flue gas; Chemical Adsorption

1 Introduction

Over the recent decades, mercury emissions from coal-fired boilers have attracted worldwide attention due to its extreme toxicity, high volatility, and strong bioaccumulation in the ecosystem¹⁻³. Mercury is treated as a hazardous and toxic pollutant according to Title III of the 1990 Clean Air Act Amendments (CAAA) in the United States⁴. Coal combustion is considered as the main anthropogenic source of mercury release on the account of the increasing world energy demands and the continual use of coal for power generation in many countries such as China and India^{5,6}. The mercury emission of new coal-fired power plants has been limited by the United States Environment Protection Agency (EPA) to 5.9 – 54.5 g/GWh⁷. Emission standards for air pollutants from coal-fired power plants in China has limited the mercury emission to 0.03 mg/m³⁸. Moreover, the Minamata Convention on Mercury for mercury restriction was signed by 140 countries in 2013 and came in to effect in 2017⁹.

There are generally existed three states of mercury species in coal combustion flue gas: the oxidized mercury (Hg²⁺), the elemental mercury (Hg⁰), and the particulate-bound mercury (Hg^p). Hg²⁺ and Hg^p can be easily captured by the wet flue gas desulfurization (WFGD) system and particulate control devices (PCDs), respectively, both of which are now the essential equipment of a modern coal-fired power plant. However, Hg⁰ is hard to be captured by the existing air pollution control devices (APCDs) due to its high volatility and insolubility¹⁰. Therefore, the key challenge to control mercury emissions from coal-fired power plants is how to effectively remove Hg⁰ from the coal-fired boiler flue gas¹¹.

Both adsorption and oxidation of Hg⁰ are deemed as the two common methods for its removal. The adsorption of Hg⁰ by use of mercury removal adsorbents has been widely applied in the lab and industrial scales. In this process, the sorbents are injected into the coal-fired flue gas to adsorb Hg⁰

directly and subsequently are removed by the APCDs. Among the adsorption-based technologies, the activated carbon injection (ACI) has been commercially used for mercury removal since 2001^{12, 13}. Activated carbons (ACs) with large specific surface areas and rich oxygen groups on the surface favour the mercury removal. It was found that the mercury removal ability of an AC could be greatly enhanced via the modification with halogen¹⁰, sulfur¹⁴, metal oxides¹⁵, and so on. However, the use of AC could adversely impede the commercial application of the fly ash due to the increasing of carbon in the ash¹⁶. To avoid such issue, many investigations on the development of non-carbon based sorbents, including mineral sorbents^{17, 18}, metal oxides sorbents¹⁹, and fly ash based sorbents^{20, 21} have been carried out in recent years. The sorbents with high specific surface areas that contribute to physisorption of Hg⁰ and abundant chemical active sites that are in favor of chemisorption and oxidation of Hg⁰ need to be developed²². Metal-organic frameworks (MOFs) with the hybrid inorganic-organic microporous crystalline, which are self-assembled straight-forwardly from metal ions with organic linkers via coordination bonds^{23, 24}, have recently attracted increasing interests due to their fascinating structures and unique properties, including high surface area, exceptional thermal stability, developed pore structures, and been applied to wastewater purification²⁵, lithium-ion battery anode²⁶, and gas storage²⁷. A number of studies have investigated the mercury removal performance over various MOFs in the recent years such as the MIL101-Cr⁴, the Br-modified UiO-66²⁸, the Cu-BTC²⁹, and the manganese-cerium loaded MOFs³⁰. All of these MOF based mercury sorbents have exhibited good Hg⁰ performance and potential to be used as substitutes for AC sorbents. Among these MOF sorbents, the MIL101-Cr (chromium terephthalate) is an attractive candidate for the mercury adsorption due to its extra-high specific surface area (approximately 2500 m²/g), good thermal stability

(decomposed more than 300 °C) and the chemical activity (the presence of Cr). Several studies have shown that Cr-containing catalysts exhibit superior catalytic activity. Chromium oxide was proved to be very active for Hg⁰ oxidation^{31,32}. Chen et al. have found that the introduction of Cr into MnOx-TiO₂ sorbents could significantly enhance their Hg⁰ removal performance in the absence and presence of SO₂³². Zhao et al. studied the Hg⁰ removal from the sintering flue gas of iron and steel over MIL101-Cr and the results showed that Hg⁰ removal efficiency could reach about 88% at 250 °C and Cr³⁺ on the surface could effectively oxidize Hg⁰⁴. However, the oxygen and moisture contents in the sintering flue gas are always higher than those in the coal-fired flue gas⁴, and the SO₂ concentration varies widely in the sintering flue gas³³. The temperature of the sintering gas is in the range of 120-180 °C²⁹, which is lower than that in the coal-fired flue gas at the down-stream of the SCR device (150-350 °C)³⁴. In addition, Zhao et al.⁴ only investigated the effect of O₂ in the flue gas on the Hg⁰ removal performance of MIL101-Cr. Both the sintering flue gas and the coal-fired boiler flue gas contain other active gaseous components such as NO, SO₂, and H₂O and the presence of these gaseous components in the flue gas can significantly affect the Hg⁰ removal performance of MIL101-Cr. Hence, to fully assess the Hg⁰ removal performance of MIL101-Cr, the investigation of the Hg⁰ removal performance must be conducted with an atmosphere containing all of the important active flue gas components (O₂, NO, SO₂, and H₂O).

In current work, the MIL101-Cr sorbent was prepared and used to remove Hg⁰ from the simulated coal-fired boiler flue gas on a fixed-bed reactor. The effects of adsorption temperature, the Hg⁰ inlet concentration, the gas hourly space velocity (GHSV) and the individual flue gas components on the Hg⁰ removal performance over the prepared MIL101-Cr were investigated systematically. The

mercury removal mechanisms and adsorption kinetics were also studied in order to further understand the Hg^0 adsorption over the MIL101-Cr sorbent, which would help to develop the promising Hg^0 removal sorbents for coal-fired power plants.

2 Experiment and computational method

2.1 Experimental section

2.1.1 Sorbents preparation

The MIL101-Cr sorbent was prepared following the well established hydrothermal method^{4, 35}. Briefly, $\text{Cr}(\text{NO}_3)_3 \cdot 9\text{H}_2\text{O}$ (16 mmol) and terephthalic acid (16 mmol) were dissolved in deionized water (100 mL) under the vigorous stirring condition to form a clear solution. Then the solution was transferred into a 200 ml Teflon-lined stainless-steel autoclave and heated at 220 °C for 18 h without stirring. After cooling to room temperature, the obtained green solid was centrifuged and washed with DMF and ethyl alcohol several times at 60 °C, and then dried in an oven at 150 °C overnight.

The commercial AC was purchased from Miaoyuan Material Co. (Gongyi, China). The commercial Br-AC was synthesized by impregnation method using NH_4Br solution. 10 g of the commercial AC were dispersed to the 1 wt.% NH_4Br solution with 12 h stirring. Then the NH_4Br -impregnated commercial AC was dried in a thermostat drying oven at 110 °C for 6 h and the commercial Br-AC was prepared finally.

2.1.2 Characterization

The powder X-ray diffraction (XRD) measurements were performed on a XD-3 X-ray diffractometer with $\text{Cu-K}\alpha$ radiation and operating at 50 kV and 200 mA (X'Pert PRO MPD, Nederland). The N_2 specific BET surface area was measured by N_2 adsorption in a constant volume adsorption apparatus

analyzer (Gold APP, China). The XPS measurements were made on a K- α spectrometer (Thermo ESCALAB 250XI, US) at room temperature under ultra-high vacuum. All binding energies of the samples were calibrated using the reference carbon (C 1s) peak at 284.8 eV.

2.1.3 Experimental method

The Hg⁰ removal tests were carried out in a fixed-bed quartz tube reactor system, as described schematically in Fig. 1. The experiment system mainly consisted of simulated flue gas supply system, mercury vapour generator, reaction temperature control system, adsorption reactor and Hg⁰ online analyzer. The simulated flue gas, including the carrier gas (N₂) for the mercury vapour, had a total flow rate of 1000 ml/min and was composed of N₂, O₂, SO₂, NO and H₂O. A flow 300 ml/min of N₂ was used as the carrier gas to convey the mercury vapour from a mercury permeation device, which was sealed in a U-shaped quartz tube and placed in a water bath to introduce a specified Hg⁰ concentration by controlling the water temperature. The Hg⁰ inlet concentration was controlled at 203 $\mu\text{g}/\text{m}^3$ with the baseline tests and was altered to 132 and 74 $\mu\text{g}/\text{m}^3$ for other specific experimental conditions. As shown in Fig. 1, the Hg⁰ carried by the carrier gas (N₂) and the flows of different gaseous components of the simulated flue gas were premixed before passing through the fixed-bed reactor. The concentration of each gaseous component in the simulated flue gas was calculated by dividing the flow rate of the gaseous component with the total flue gas flow rate after the mixing chamber. The adsorption tests were conducted by packing 50 mg sorbents (with particles of 40-60 meshes) into a quartz glass tube reactor (i.d. 8 mm) that was placed in a temperature-controlled furnace. The GHSV under the baseline test condition was about $8 \times 10^5 \text{ h}^{-1}$. The GHSV was set at different values by using various amounts of sorbents (25 mg, 100 mg and 200 mg) for better understanding the influence of

GHSV on the Hg^0 removal performance. The Hg^0 concentration of the outlet gas was detected by an online continuous vapour-mercury analyzer with the accuracy of 0.1 ug/m^3 and the detection limit of 0.1 ug/m^3 (VM3000, Mercury Instruments, Germany). The vent gas was purified using activated carbon and sodium hydroxide solution to avoid air pollution. At the beginning of each test, the gas containing Hg^0 was first passed through a bypass quartz tube without adsorbents to stabilize the mercury concentration. When the concentration of Hg^0 fluctuated within $\pm 5\%$ for more than 30 min, the gas was diverted to the reactor tuber which contained the sorbents. All the gas flow lines were kept at about $110 \text{ }^\circ\text{C}$ by use of heating tapes to avoid the condensation of gaseous Hg^0 and water vapour. The impingers containing NaOH aqueous solution and silicone gel were located before the mercury analyzer inlet to avoid the corrosion of the analyzer caused by the acid gases and water vapour. In order to investigate the Hg^0 adsorption and oxidation behavior during the Hg^0 removal process over MIL101-Cr, a mercury speciation conversion system which included two impingers contained either a KCl solution (side I) or a 10% $SnCl_2/HCl$ solution (side II) was used and placed between the NaOH impinger and the silicone gel impinger (Fig. 1). When the simulated flue gas passed through side I, the Hg^{2+} (Hg_{out}^{2+}) was captured by KCl solution and only the Hg^0 (Hg_{out}^0) was measured by the VM3000. When the flue gas passed through side II, gaseous Hg^{2+} was reduced to Hg^0 , and the total mercury concentration ($Hg_{out}^T = Hg_{out}^0 + Hg_{out}^{2+}$) was determined by the mercury analyzer (VM3000). The total Hg^0 removal efficiency (E_T), Hg^0 adsorption efficiency (E_{ads}) and the Hg^0 oxidation efficiency (E_{oxi}) were calculated using following equations (1-3):

$$E_T = \frac{\sum_0^t Hg_{in}^0 - \sum_0^t Hg_{out}^0}{\sum_0^t Hg_{in}^0} \times 100\% \quad (1)$$

$$E_{\text{ads}} = \frac{\sum_0^t Hg_{\text{in}}^0 - \sum_0^t Hg_{\text{out}}^T}{\sum_0^t Hg_{\text{in}}^0} \times 100\% \quad (2)$$

$$E_{\text{oxi}} = \frac{\sum_0^t Hg_{\text{out}}^T - \sum_0^t Hg_{\text{out}}^0}{\sum_0^t Hg_{\text{in}}^0} \times 100\% \quad (3)$$

where Hg_{in}^0 donates the inlet Hg^0 concentration ($\mu\text{g}/\text{m}^3$), Hg_{out}^0 donates the outlet Hg^0 concentration ($\mu\text{g}/\text{m}^3$), and Hg_{out}^T donates the outlet total mercury concentration ($\mu\text{g}/\text{m}^3$). t donates the adsorption time (min).

The accumulative Hg^0 adsorption capacity q_t ($\mu\text{g}/\text{g}$) could be calculated by the following equation:

$$q_t = \frac{1}{m} \int_0^t (Hg_{\text{in}}^0 - Hg_{\text{out}}^0) \times Q dt \quad (4)$$

where Q represents the total gas flow rate (m^3/min) and m represents the sorbent mass (g).

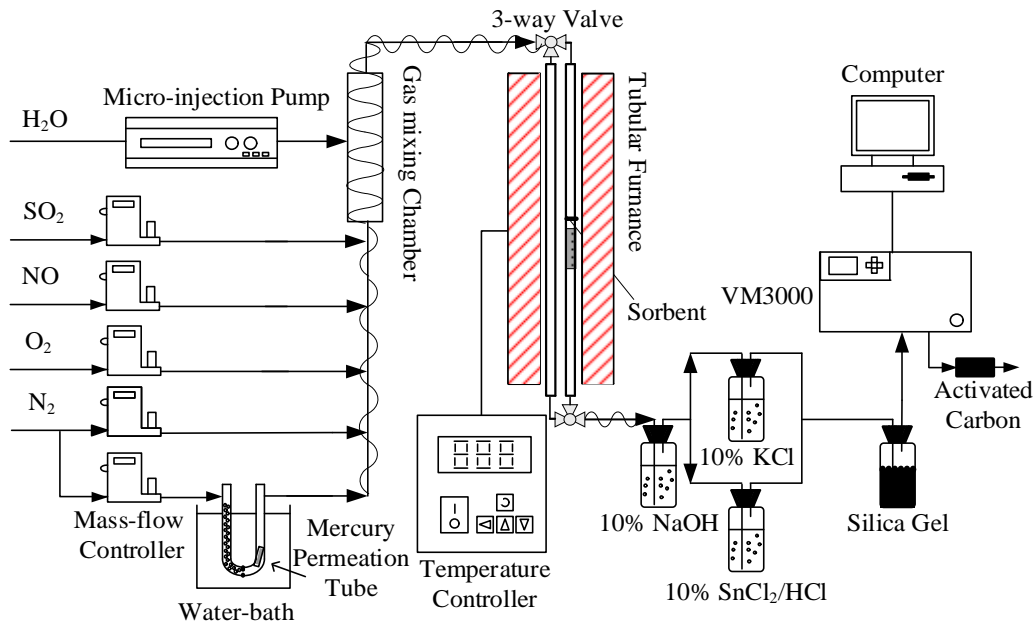


Fig. 1 Schematic diagram of the fixed-bed reactor system.

3 Results and discussion

3.1 Sample characterization

The XRD patterns of the prepared MIL101-Cr sample are shown in Fig. 2. The characteristic peaks at 5.16° , 8.50° , 5.62° , 5.92° and 9.12° are consistent with the peak locations and relative intensities reported for MIL101-Cr³⁶, suggesting the successful preparation of the MIL101-Cr sample.

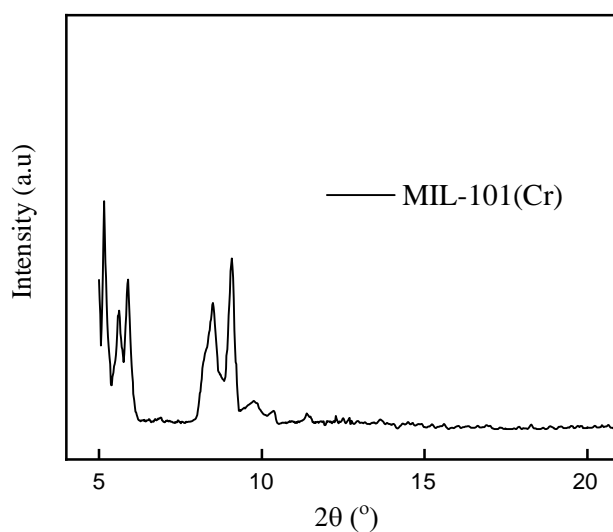


Fig. 2 XRD patterns of the prepared MIL101-Cr sorbent.

The nitrogen adsorption isotherm of the prepared MIL101-Cr sorbent is showed in Fig. 3. The MIL101-Cr sorbent has presented the type-IV adsorption isotherm, according to the IUPAC classification, indicating that the sample has a mesoporous structure which is beneficial to mercury removal³⁷. The BET specific surface area and total pore volume of the sample is $2368 \text{ m}^2/\text{g}$ and $1.48 \text{ cm}^3/\text{g}$, respectively.

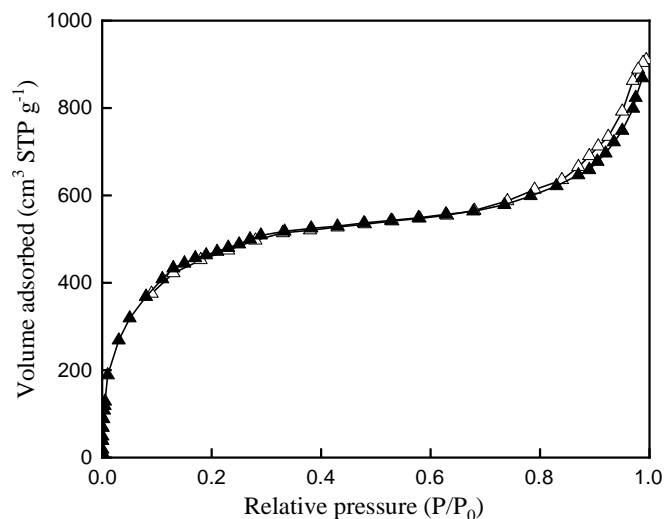


Fig. 3 N₂ adsorption-desorption isotherms of MIL101-Cr sorbent.

3.2 Activity performance

3.2.1 Hg⁰ removal performance

Fig. 4 shows the Hg⁰ removal efficiencies of the MIL101-Cr sample within the reaction temperature range of 50-300 °C under the atmosphere of N₂+5% O₂. It can be seen that the average Hg⁰ removal efficiency within 4 h increased with the reaction temperature, increasing from 50.2% at 50 °C to 85.5% at 200 °C. When the temperature was higher than 200 °C, the mercury removal performance became deteriorated with the reaction temperature: the average Hg⁰ removal efficiency was 78.5% at 250 °C and 70.2% at 300 °C, respectively. The adsorption of Hg⁰ on the surface of the MIL101-Cr sorbents is a combination of physisorption and chemisorption. The adsorption of Hg⁰ through physisorption is favoured at a lower temperature, whereas the chemisorption is related to activation energy and proceeds at a limited rate which increases with the temperature increasing³⁸. Hence, a higher reaction temperature is beneficial to the chemisorption. At the temperature of 50 °C, only physisorption could have occurred; however, the total Hg⁰ removal efficiency was not very low (50.2%) due to the high

BET surface area ($2368 \text{ m}^2/\text{g}$) which can provide more adsorption sites. Since physisorption is easy to reach saturation, the Hg^0 adsorption of the MIL101-Cr sorbent at $50 \text{ }^\circ\text{C}$ was quite close to breakthrough after the 4 h reaction. At higher temperatures, both physisorption and chemisorption contribute to the Hg^0 adsorption. However, when the reaction temperature was increased from $200 \text{ }^\circ\text{C}$ to $250 \text{ }^\circ\text{C}$ and $300 \text{ }^\circ\text{C}$, the Hg^0 removal ability of the sorbent was seen clearly decreasing with the temperature, which can be attributed to the release of the surface-bound mercury species and the decomposition of mercury oxide^{39, 40}. From the above results, it can be seen that $200 \text{ }^\circ\text{C}$ was the best operating temperature for Hg^0 removal over MIL101-Cr, and hence this temperature was selected for the subsequent studies of the Hg^0 removal performance.

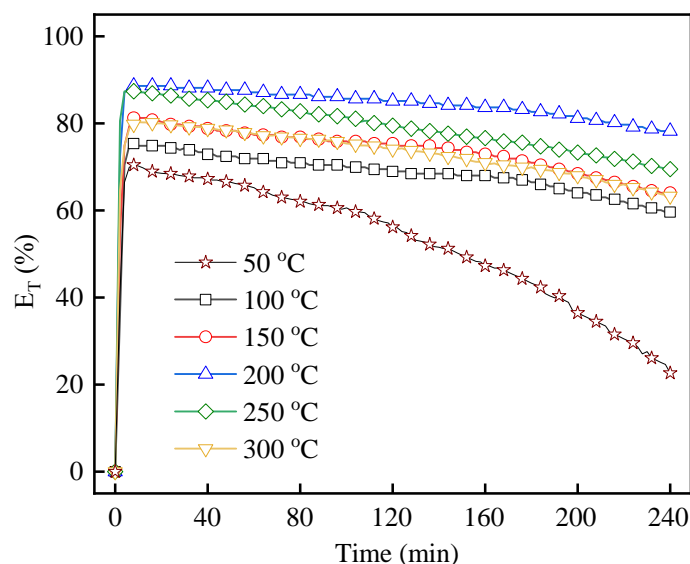


Fig. 4 Hg^0 removal efficiency over the MIL101-Cr sorbent.
(Reaction condition: $\text{N}_2+5\% \text{ O}_2$, $203 \mu\text{g}/\text{m}^3$, $8 \times 10^5 \text{ h}^{-1}$)

3.2.2 Effect of inlet Hg⁰ concentration and GHSV

It should be noted that the inlet concentration of Hg⁰ at 203 µg/m³ in the tests of Fig.4 is far higher than the values in other researchers' investigations^{4, 17}. Hence, the inlet concentration of Hg⁰ was reduced to 132 and 74 µg/m³ in order to study its effects on Hg⁰ removal performance over MIL101-Cr. As shown in Fig. 5, higher mercury removal efficiencies (88.8% and 92.5%, respectively) were achieved at these lower Hg⁰ concentrations. Decreasing the inlet Hg⁰ concentration led to the decrease of the number of mercury molecules through the reactor. Hence, the relative molar ratio of the sorbent to mercury was increased, benefitting the mercury removal⁴¹. It can be inferred that a very high mercury removal efficiency can be acquired with the MIL101-Cr sorbent in the actual coal-fired flue gas as the mercury concentration in the actual coal-fired flue gases is only ranged from 3 to 30 µg/m³, which is much lower than that used in this study.

The GHSV is a crucial parameter for the mercury adsorption performance of sorbents. The effect of GHSV on the Hg⁰ removal efficiency over the MIL 101-Cr sorbent tested was experimentally investigated and the results are shown in Fig. 5. It can be observed that the Hg⁰ removal efficiency decreased to 65.6% from 85.5% when the GHSV increased to $1.6 \times 10^6 \text{ h}^{-1}$ from $8 \times 10^5 \text{ h}^{-1}$. An elevated GHSV could lead to a shorter residence time of the mercury containing flue gas in the sorbent, resulting in a shorter contact and adsorption time between the mercury and the sorbent. Similar to the results of other studies^{41, 42}, a better mercury removal performance was acquired when the GHSV was decreased due to a longer residence time between the mercury and the sorbent. The mercury removal efficiency reached to almost 98% when the GHSV decreased to $2 \times 10^5 \text{ h}^{-1}$. It is worth noting that the GHSV ($8 \times 10^5 \text{ h}^{-1}$) investigated in this study are much higher compared to other researches^{41, 42}.

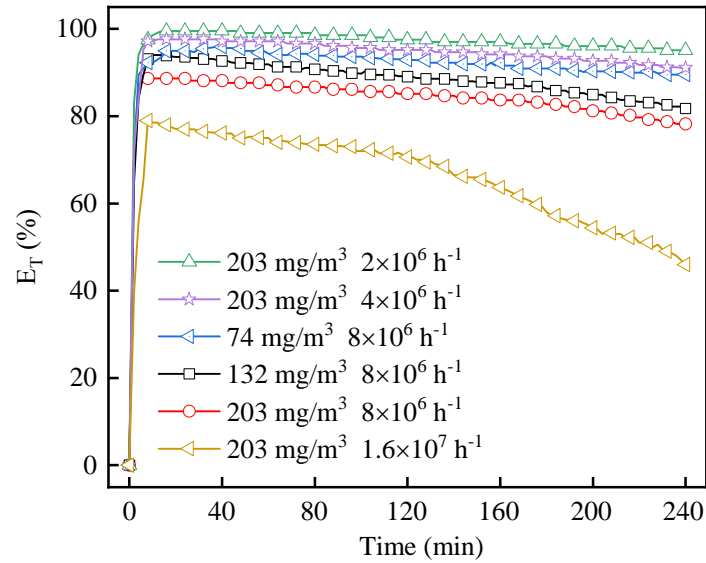


Fig. 5 Effect of inlet Hg^0 concentration and GHSV on the Hg^0 removal performance. (Reaction condition: $\text{N}_2+5\% \text{O}_2$, 200 °C)

3.2.3 Effect of individual flue gas component

3.2.3.1 Effect of O_2

O_2 is an indispensable flue gas component and could play an essential role in Hg^0 adsorption reaction. The effect of O_2 in the flue gas on the mercury removal performance of the MIL101-Cr sorbent (at 200 °C) was experimentally investigated with the flue gases containing different O_2 concentrations, and the results are shown in Fig. 6. Fig. 6 clearly shows that the MIL101-Cr sample had a poor performance of Hg^0 removal with the flue gas containing no O_2 , and its Hg^0 removal efficiency decreased to lower than 40.0% after 4 h adsorption reactions. When the O_2 content in the flue gas increased from 0 to 5% and 10%, the average Hg^0 removal efficiency of the MIL101-Cr increased from 60.5% to 85.5% and 88.1%, respectively. This indicates that an increase in the O_2 concentration could effectively enhance the Hg^0 adsorption performance over the MIL101-Cr sorbent. The gas-phase O_2 in flue gas could replenish and regenerate the consumed surface oxygen on the adsorbent surface, which serves as the oxidant consumed in the Hg^0 oxidation process, thus enhancing

the Hg^0 removal^{43,44}. The results in Fig. 6 also show that the Hg^0 removal efficiency at 10% O_2 was only slightly higher (2.6%) than that at 5% O_2 , implying 5% O_2 in the flue gas was enough for regenerating and replenishing the consumed surface oxygen.

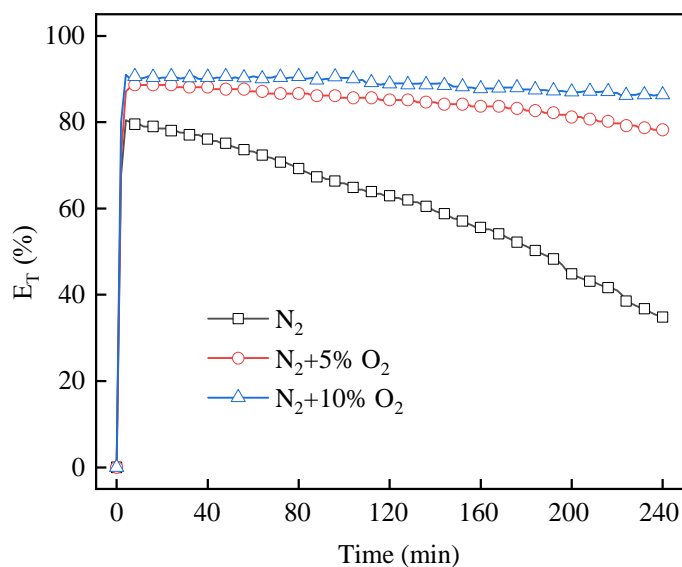
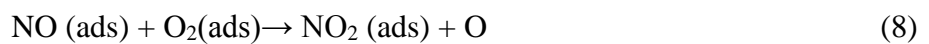
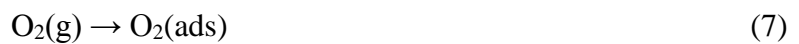
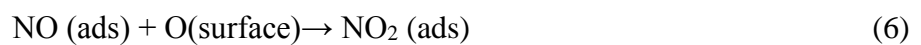
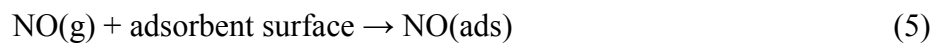


Fig. 6 Effect of O_2 concentration on the Hg^0 removal performance.
(Reaction condition: $203 \mu\text{g}/\text{m}^3$, $8 \times 10^5 \text{ h}^{-1}$, $200 \text{ }^\circ\text{C}$)

3.2.3.2 Effect of NO

NO is one of the main pollutants present in component of coal-fired boiler flue gases. Therefore, Hg^0 removal experiments with the MIL101-Cr sorbent were carried out with the flue gases containing different concentrations of NO. The results shown in Fig. 7 indicate that NO in the flue gas facilitated the Hg^0 removal both in the absence and presence of O_2 . Compared with the Hg^0 removal performance over the MIL101-Cr sorbent without NO in the pure N_2 , the addition of 200 ppm NO greatly enhanced the Hg^0 removal ability, the average efficiency having increased from 61.5% to 87.2%. Besides, with the help of 5% O_2 , the presence of 200 ppm NO in the flue gas resulted in the Hg^0 removal efficiency to achieve to 93.8%. With further increases of the NO concentration to 600 ppm and 1200 ppm, the Hg^0 removal efficiency still maintained at about 95.0%. It has been reported that the presence of NO

could produce the active species such as NO₂, NO⁺ on the surface of the metal based sorbents^{17, 45}, which can facilitate the oxidation removal of Hg⁰. From Fig. 7, it can also be seen that the Hg⁰ removal efficiency of MIL101-Cr with the flue gas containing both O₂ and NO was higher than that with the flue gas only having the presence of the NO alone. This can be attributed to the following: in the presence of O₂, more adsorbed NO could be oxidized on the sorbent to form abundant active species like NO₂, at the same time, the gas phase O₂ could also regenerate the consumed surface oxygen species²¹. The surface chemistry of the used MIL101-Cr sorbent, which had captured the Hg⁰ included in the atmosphere of N₂+5% O₂+600 ppm NO, was investigated by XPS analysis to identify the nitrogen species on the surface of the sorbent. As shown in Fig. 8, a small peak of the N 1s spectra appeared at 406.0 eV which can be attributed to NO₂ and a big peak appeared at 400.0 eV which can be assigned to NO₃⁻ on the surface of the MIL101-Cr sorbent⁴⁶. This confirms that NO₂ was produced by the reaction of the NO containing flue gases with the sorbent, and subsequently participated in the Hg⁰ oxidation process to form Hg(NO₃)₂. The reactions involved in these processes can be described as follows (5-11).



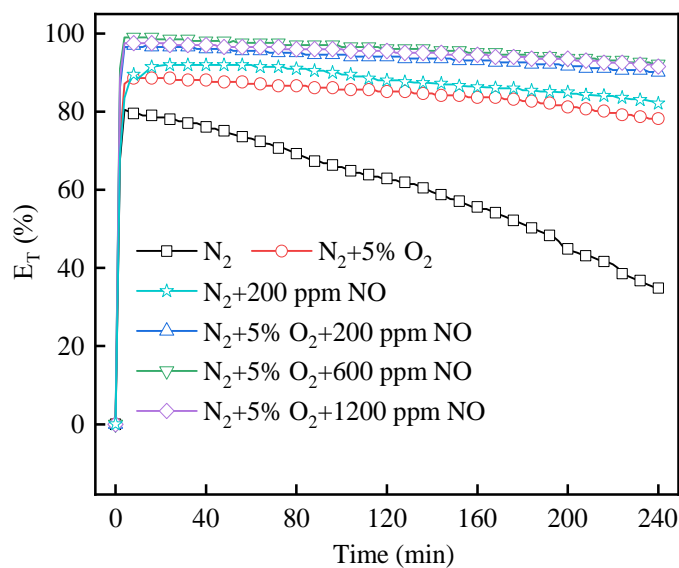


Fig. 7 Effect of NO concentration on the Hg⁰ removal performance. (Reaction condition: 203 μg/m³, 8 × 10⁵ h⁻¹, 200 °C)

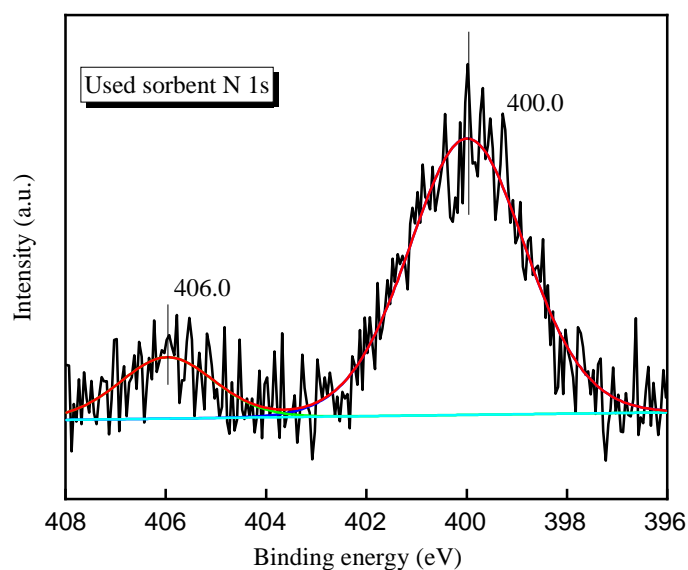


Fig. 8 XPS spectra of the used MIL101-Cr sorbent over the N 1s spectral.

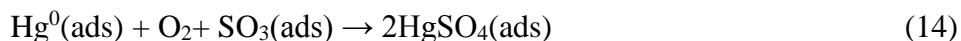
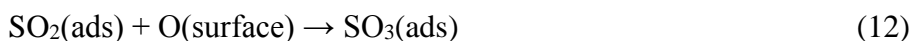
(Reaction condition: N₂+5% O₂+ 600 ppm NO, 203 μg/m³, 8 × 10⁵ h⁻¹, 200 °C, 2 h)

3.2.3.3 Effect of SO₂

As another main pollutant present in coal-fired boiler flue gases, SO₂ has been proved to play an crucial role in Hg⁰ removal process over many sorbents^{32, 39, 40}. The effect of the SO₂ in the flue gas on the performance of Hg⁰ removal over the MIL101-Cr sorbent used in this study is shown in Fig. 9.

The presence of SO₂ in the flue gas had an obvious inhibiting effect on the Hg⁰ removal. When 200 ppm SO₂ was introduced to the pure N₂ gas stream, the average Hg⁰ removal efficiency within 4 h decreased from 61.5% to 39.8%, which could be ascribed to the consumption of the surface active oxygen species by the reaction of SO₂ (Eq. 12) and the competitive adsorptions between SO₂ and Hg⁰ for the surface active sites⁴⁷. In order to further prove the competitive adsorptions between SO₂ and Hg⁰, the desorption experiment was carried out following the procedure shown in Fig. 10. The MIL101-Cr sample was first pretreated under the condition of Hg⁰+N₂ at 200 °C for 60 min, then the feeding of Hg⁰ was cut off and the mercury-loaded sample was purged in N₂ for 30 min to remove the surface weakly adsorbed mercury. After the N₂ purging, 1200 ppm SO₂ was added to the simulated flue gas (pure N₂ in this case). The results in Fig. 10 clearly show that the Hg⁰ concentration at the exit of the reactor increased immediately when SO₂ was introduced to the flue gas, increasing from about 0 to 54.2 µg/m³. This suggests that the introduced SO₂ had replaced the surface bond mercury, i.e. made part of the surface mercury desorb at 200 °C, indicating the competitive adsorptions of SO₂ and Hg⁰ would occur over the MIL101-Cr sorbent. The results in Fig. 9 show that the presence of 5% O₂ in the flue gas had significantly weakened the inhibiting effect of SO₂ on the Hg⁰ removal efficiency which was still higher than 71.0% after 4 h adsorption under the conditions of 5% O₂ plus 200 ppm SO₂. This can be attributed to the beneficial effect of O₂ on the oxidation of Hg⁰, and the replenishment and regeneration of the consumed surface oxygen by the gaseous O₂. Besides, SO₂ can react with O₂ to produce SO₃⁴⁰, which is favourable to the chemisorption of Hg⁰ (Eqs. 13-14). Therefore, a low concentration of SO₂ (200 ppm) with the presence of 5% O₂ slightly impeded the Hg⁰ removal by the MIL101-Cr sorbent. However, further increasing the SO₂ concentration in the flue gas to 600 ppm and

1200 ppm resulted in much lower Hg⁰ average removal efficiency within 4 h, to 53.5% and 45.1% (Fig.8), respectively. The reduction of Hg⁰ removal performance could be explained by the inhibition effects of competitive adsorption between SO₂ and Hg⁰ and the surface sulfation of MIL101-Cr, which could counteract the promotion of SO₃ for the oxidization of Hg⁰ ¹⁷. In order to verify if SO₂ had reacted with the MIL101-Cr leading to the reduction of its Hg⁰ removal ability, the Hg⁰ removal experiment over the SO₂ pretreated sorbent was performed and the results are shown in Fig. 11. The MIL101-Cr sorbent was first pretreated with 1200 ppm SO₂ under the N₂+5% O₂ atmosphere at 200 °C for 60 min before the Hg⁰ adsorption test in order to eliminate the effect of competitive adsorptions between SO₂ and Hg⁰. It can be observed from Fig. 11, that the Hg⁰ removal efficiency over the SO₂ pretreated MIL101-Cr sorbent was much lower than that of the fresh MIL101-Cr sorbent. This confirms the assumption that SO₂ could react with the MIL101-Cr resulting in the formation of inactivative species such as sulfate species which would impair the Hg⁰ removal ability. The surface chemistry of the used MIL101-Cr sorbent, which was pretreated with N₂+5% O₂+1200 ppm SO₂, was identified by XPS to ascertain this inference. As shown in Fig. 12, the S 2p peaks mainly centered at 168.9 eV, which is attributed to SO₄²⁻. This further indicates that SO₂ can react with the MIL101-Cr sorbent to form sulfate, which is detrimental to Hg⁰ removal.



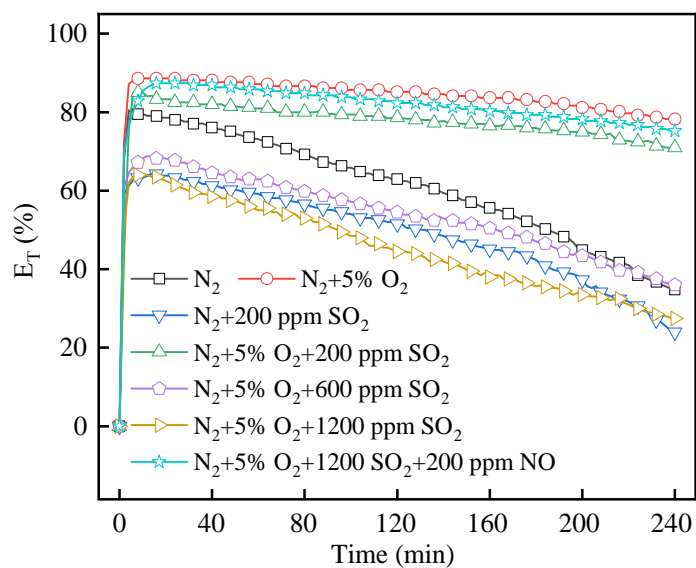


Fig. 9 Effect of SO_2 concentration on the Hg^0 removal performance. (Reaction condition: $203 \mu\text{g}/\text{m}^3$, $8 \times 10^5 \text{ h}^{-1}$, $200 \text{ }^\circ\text{C}$)

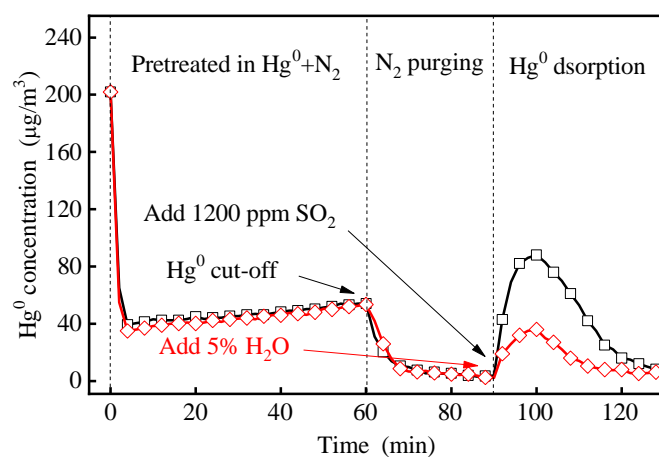


Fig. 10 Hg^0 desorption by SO_2 or H_2O over MIL101-Cr at $200 \text{ }^\circ\text{C}$. (Reaction condition: $8 \times 10^5 \text{ h}^{-1}$, $200 \text{ }^\circ\text{C}$)

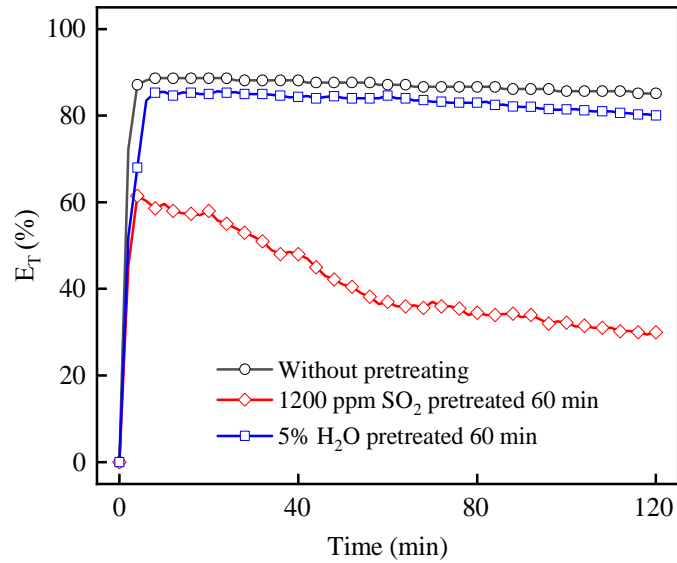


Fig. 11 Hg^0 removal performance over the SO_2 or H_2O pretreated MIL101-Cr.

(Reaction condition: $N_2+5\% O_2$, $203 \mu g/m^3$, $8 \times 10^5 h^{-1}$, $200 \text{ }^\circ C$)

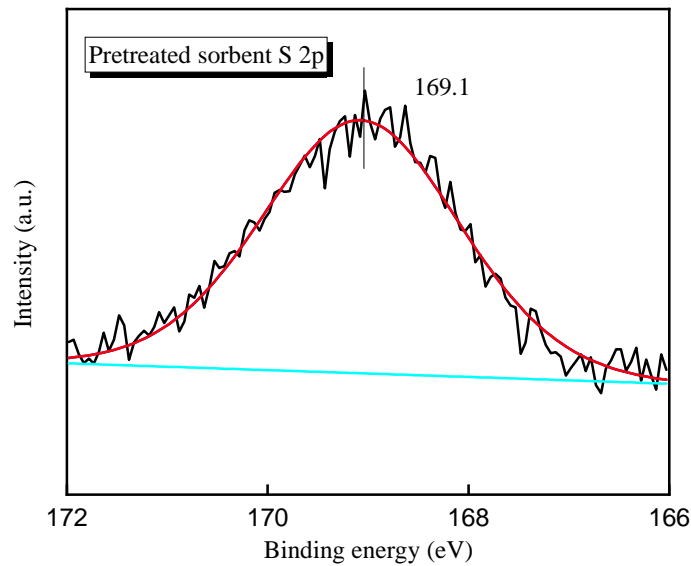


Fig. 12 XPS spectra of the pretreated MIL101-Cr sorbent over the S 2p spectral.

(Reaction condition: $N_2+5\% O_2+1200 \text{ ppm } SO_2$, $8 \times 10^5 h^{-1}$, $200 \text{ }^\circ C$, 2 h)

As depicted in section 3.2.3.2, the presence of NO could enhance the Hg^0 removal over the MIL101-Cr sorbent. Therefore, the effects of the simultaneous presence of 200 ppm NO and 1200 ppm SO_2

on the Hg^0 adsorption whereas also investigated in this study and the results, also shown in Fig. 9, clearly indicate that the inhibition effect of SO_2 on the Hg^0 removal activity was greatly alleviated by the introduction of NO. The Hg^0 removal efficiency reached 81.3% when 200 ppm NO and 1200 ppm SO_2 were introduced to $\text{N}_2+5\% \text{O}_2$, which was much higher than that was achieved with the flue gas of $\text{N}_2+5\% \text{O}_2+1200 \text{ ppm SO}_2$. This can be partly ascribed to the formation of NO^+ and NO_2 as a result of the introduction of NO, and partly due to the oxidization of SO_2 to SO_3 by NO_2 and O_2 . As NO always exists in the actual coal-fired flue gas, NO can partly offset the inhibitory effect of SO_2 on the Hg^0 removal by the sorbent.

3.2.3.4 Effect of H_2O

H_2O always exists in real flue gases. Thus, the effect of H_2O in the flue gas on Hg^0 removal was investigated in this study. From Fig. 13, it can be seen that the Hg^0 removal efficiency decreased from 87.1% to 81.4% when 5% of H_2O was added. After 60 min reaction, the Hg^0 removal efficiency was slightly reduced to 78.4%, whereas the efficiency increased to 83.6% when the water vapour was cut off. The results indicate that the presence of H_2O in the flue gas negatively affected the mercury removal performance over the MIL101-Cr. This is largely due to the competitive adsorptions between H_2O and Hg^0 and/or the H_2O vapour covering the active adsorption sites for Hg^0 ^{48, 49}. The Hg^0 desorption experiment and the Hg^0 adsorption experiment with the 5% H_2O pretreated sorbent similar to those described in section 3.2.3.3 were performed to ascertain these two effects as shown in Figs. 10 and 11. It can be seen from Fig. 10 that a spike of Hg^0 was appeared after adding 5% H_2O due to the desorption of the surface adsorbed mercury. However, as shown in Fig. 11, the Hg^0 removal efficiency with the 5% H_2O pretreated sorbent was almost as high as that of the fresh sorbent,

indicating the MIL101-Cr sorbent pretreated with 5% H₂O has insignificant impact on the Hg⁰ removal ability. Therefore, it can be concluded that the competitive adsorption instead of the surface site deactivation was responsible for the reduced adsorption ability when H₂O was present in the flue gas.

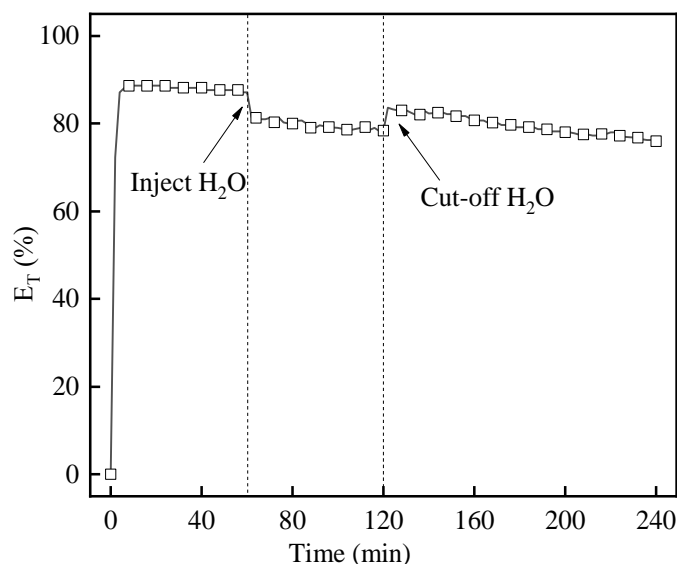


Fig. 13 Effect of H₂O concentration on the Hg⁰ removal performance.
(Reaction condition: N₂+5% O₂, 203 μg/m³, 8 × 10⁵ h⁻¹, 200 °C)

3.2.4 Comparison of the Hg⁰ adsorption capacity between MIL101-Cr and commercial AC

In order to compare the Hg⁰ removal performance of the MIL101-Cr sorbent with that of a standard Hg⁰ adsorbent, the commercial Br-AC was selected and used to remove Hg⁰ under the same reaction conditions. As shown above, O₂, SO₂, NO and H₂O in the coal-fired flue gas have various effects on the Hg⁰ removal performance of the MIL101-Cr sorbent. Hence, the simulated flue gas (SFG) containing 5% O₂, 200 ppm NO, 1200 ppm SO₂ and 5% H₂O, balanced with N₂, was used for the Hg⁰ removal performance with the MIL101-Cr sorbent and commercial Br-AC at the optimal reaction temperature of 200 °C. As shown in Fig. 14 (a) for the MIL101-Cr sorbent, the Hg⁰ removal performance under the SFG atmosphere was only slightly worse than that under the atmosphere of

$\text{N}_2+5\% \text{O}_2$. The results shown above that already confirmed both SO_2 and H_2O had inhibiting effects on the mercury removal performance, while NO could enhance the Hg^0 removal ability. Hence, the presence of NO in the flue gas can counteract the adverse effects of SO_2 and H_2O . Under the same SFG atmosphere the commercial Br-AC had a much worse Hg^0 removal performance in comparison with the MIL101-Cr sorbent (Fig. 14 (a)). After 240 min reactions, the mercury removal efficiency of the commercial Br-AC decreased to 28.4%, while the Hg^0 removal efficiency of the MIL101-Cr sorbent maintained above 70%. This means that the commercial Br-AC almost reached the mercury adsorption saturation after 240 min, whereas the MIL101-Cr sorbent still had the good ability to further adsorb mercury. The accumulated mercury adsorption capacities (q_t) at 240 min were calculated according to Eq. 4 and are shown in Fig. 14 (b). It can be seen that the q_t value of the commercial Br-AC under the SFG condition was only $472.2 \mu\text{g/g}$, while for the MIL101-Cr sorbent, the q_t value reached $770.2 \mu\text{g/g}$, which was over 60% higher than that of the commercial Br-AC. As will be shown in Section 3.3.3, the equilibrium mercury adsorption capacity of the MIL101-Cr sorbent can be calculated to be as high as $25656 \mu\text{g/g}$. The comparison of the mercury adsorption capacity between the MIL101-Cr sorbent and other sorbents evaluated by other researchers is presented in Table 1. Clearly, the MIL101-Cr sorbent evaluated in this study can be considered as an outstanding mercury sorbent due to its largest specific surface area, excellent mercury removal efficiency and high mercury adsorption capacity.

Although it is true that the synthetic cost of the MIL101-Cr sorbent is higher than that of the commercial Br-AC, it should be noted that introducing a magnetic medium (such as Fe_3O_4 or $\gamma\text{-Fe}_2\text{O}_3$) into this MOF material can make this sorbent magnetic and hence become re-useable and recyclable.

These kinds of magnetic MOF materials have been applied into the fields of organophosphate esters sorption⁵⁰ and luminol chemiluminescence catalysis⁵¹, and can also be applied as efficient and economic magnetic mercury sorbents for Hg⁰ removal from coal-fired boiler flue gases.

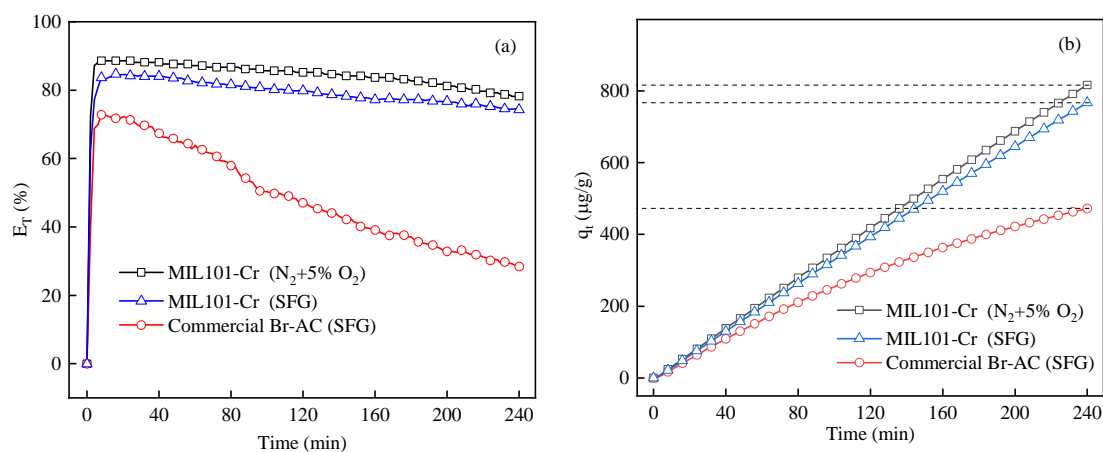


Fig. 14 Hg⁰ removal efficiencies (a) and adsorption capacities (b) of MIL101-Cr and commercial Br-AC. (Reaction condition: 203 µg/m³, 8 × 10⁵ h⁻¹, 200 °C)

Table 1 Comparison of Hg⁰ adsorption capacity of the MIL101-Cr with other sorbents.

Sorbents	Adsorption temperature (°C)	BET surface area (m ² /g)	q _e (µg/g)	References
Fe _{1.5} MBC ₆₀₀	150	657.24	1279.6	52
S8Br5	160	19.66	952.4	10
Br-CAC	145	438	585.0	38
FC-20	150	42.43	473.93	53
T6W1P1	140	17.5	353.36	5
MIL101-Cr	200	2368	25656	This work

3.3 Discussion on the mechanism of Hg⁰ removal

3.3.1 Identification of the Hg⁰ adsorption and oxidation behaviors over MIL101-Cr

The Hg⁰ adsorption and oxidation behaviors over the MIL101-Cr sorbent were studied by using the mercury speciation conversion system. As it can be seen from Fig. 15 (a), when Hg⁰ was passing through the MIL101-Cr sorbent, the outlet Hg⁰ and Hg^T concentrations decreased from 203 µg/m³ to 44.2 µg/m³ and 59.5 µg/m³ after 240 min reaction at 200 °C, respectively. The difference between the Hg^T and Hg⁰ concentrations, which can be defined as the concentration of Hg²⁺, increased gradually

with the reaction time, reaching to $13.3 \mu\text{g}/\text{m}^3$ after 4 h of reaction. This indicates that the most mercury species, included Hg^0 and/or Hg^{2+} , were retained on the surface of the MIL101-Cr sorbent. Fig. 15 (b) shows the Hg^0 adsorption and oxidation efficiencies over the MIL101-Cr sorbent at various reaction temperatures (50-300 °C). At 50 °C, almost no Hg^{2+} was observed at the outlet of the flue gas as the low temperature inhibited the oxidation of Hg^0 . It can be observed from Fig. 15 (b) that the variation trend of the Hg^0 adsorption efficiency (E_{ads}) is the same as the Hg^0 removal efficiency (E_{T}). As the reaction temperature was increased from 100 °C to 300 °C, the Hg^0 oxidation efficiency (E_{oxi}) increased from 1.9% to 13.5%, indicating more Hg^0 being oxidized at the elevated reaction temperature. However, the Hg^0 oxidation efficiency was still very low in comparison to the E_{ads} at various reaction temperatures. At the temperature of 200 °C in this study, the E_{ads} and the E_{oxi} were 81.6% and 3.9%, respectively. Hence, it can be concluded that the chemical adsorption of Hg^0 was the dominant mechanism in the Hg^0 removal process. The Hg^0 removal process over the MIL101-Cr sorbent belongs to the chemisorption reaction rather than to the heterogeneous catalysis.

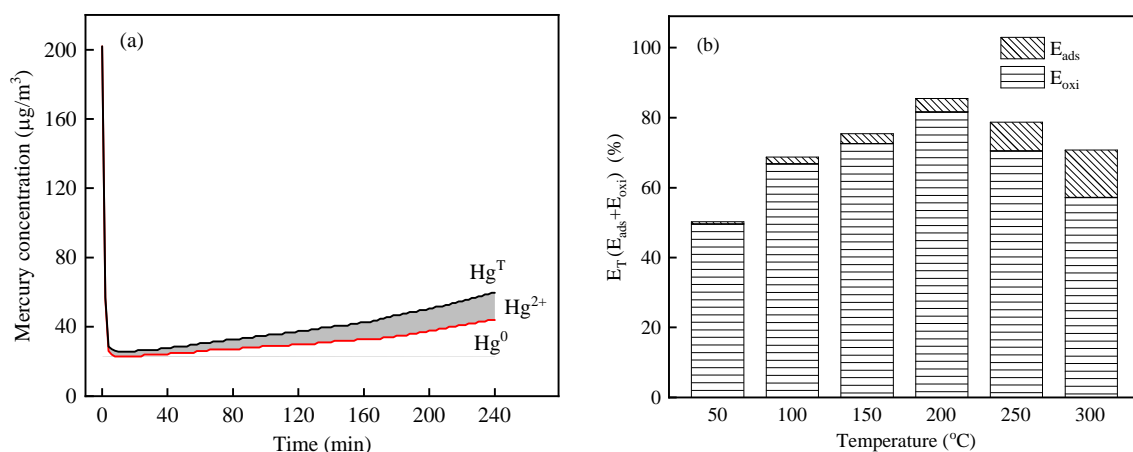


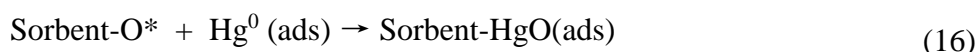
Fig. 15 (a) The outlet Hg^0 , Hg^{2+} , and Hg^{T} concentrations under the reaction temperature of 200 °C; (b) Hg^0 adsorption and oxidation efficiency at various reaction temperatures.

(Reaction condition: 203 $\mu\text{g}/\text{m}^3$, $8 \times 10^5 \text{ h}^{-1}$)

3.3.2 XPS analysis

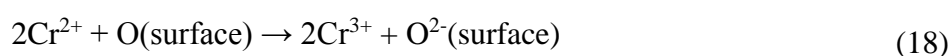
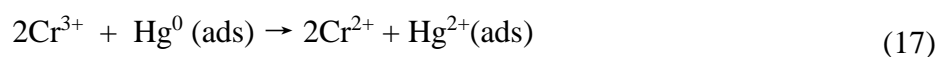
To further understand the mechanism of Hg^0 removal by the MIL 101-Cr sample, the chemistry valence of the elements on the surface of the MIL 101-Cr sample was determined by the XPS technique. The XPS spectra of Cr 2p, C 1s, O 1s and Hg 4f for the fresh and used MIL101-Cr samples are shown in Fig. 16. The surface atomic concentrations and surface atomic ratios based on the XPS results are summarized in Table 2.

The XPS spectra of O 1s for the fresh and used samples are shown in Fig. 16 (a). It can be seen that three different oxygen peaks were observed on both samples. The peak at about 530.2 eV was attributed to lattice oxygen (O^{2-})⁴, and the peak at about 531.5 eV was assigned to the chemisorbed oxygen and/or weakly bonded oxygen species (O^*)⁵⁴. The third peak at around 533.0 eV was related to the generation of C-O^{52, 55}. After Hg^0 adsorption tests, the content of O^{2-} increased from 70.2% to 77.5%, while the content of O^* decreased from 23.4% to 10.3% (Table 2). The decreasing of O^* in the used MIL101-Cr indicated that O^* participated in the Hg^0 removal reaction. The increasing of O^{2-} in the used MIL101-Cr sample could be due to the appearance of O^{2-} in HgO (Eqs. 15-16)⁵². Furthermore, the increase of C-O might be due to some active O^* species being transformed into C-O groups during the process of Hg^0 removal¹⁰.



From the XPS spectra of Cr 2p shown in Fig. 16 (b), it can be seen that two peaks centered at about 577.1 eV and 586.7 eV ascribed to Cr^{3+} ⁵⁶. A weak peak belonging to Cr^{2+} could be observed for the used MIL101-Cr sorbent at the binding energy of 576.3 eV⁴. According to previous research, the Cr^{3+}

on the surface could reduce to Cr^{2+} during the process of Hg^0 oxidization. But in the presence of O_2 , Cr^{2+} could be oxidized to Cr^{3+} again by the surface chemisorbed oxygen. The intensity for Cr 2p peaks became weaker after the reaction, indicating the combination of Cr sites and mercury species occurred during the Hg^0 removal process. The involving pathways of the Hg^0 oxidization in relate to $\text{Cr}^{3+}/\text{Cr}^{2+}$ and oxygen species could be described as follows (Eqs. 17-18).



The XPS spectra of C 1s in the fresh and spent samples are shown in Fig. 16 (c). The curves of C 1s region can be deconvoluted into three peaks located at around 284.8 eV, 286.1 eV and 288.8 eV, which can be attributed to C-C binding, C-O binding, and C=O binding⁵². After the adsorption of Hg^0 , the content of C=O groups was decreased from 14.1% to 6.6%. In contrast, the content of C-O groups was increased from 15.5% to 26.6%. The results indicate that the C=O groups might be converted into the C-O groups in the process of Hg^0 removal. The C=O groups could act as the electrons' acceptor during the Hg^0 oxidization process and facilitate the electron transfer⁵⁷, which could be interpreted as reactions 19 and 20.



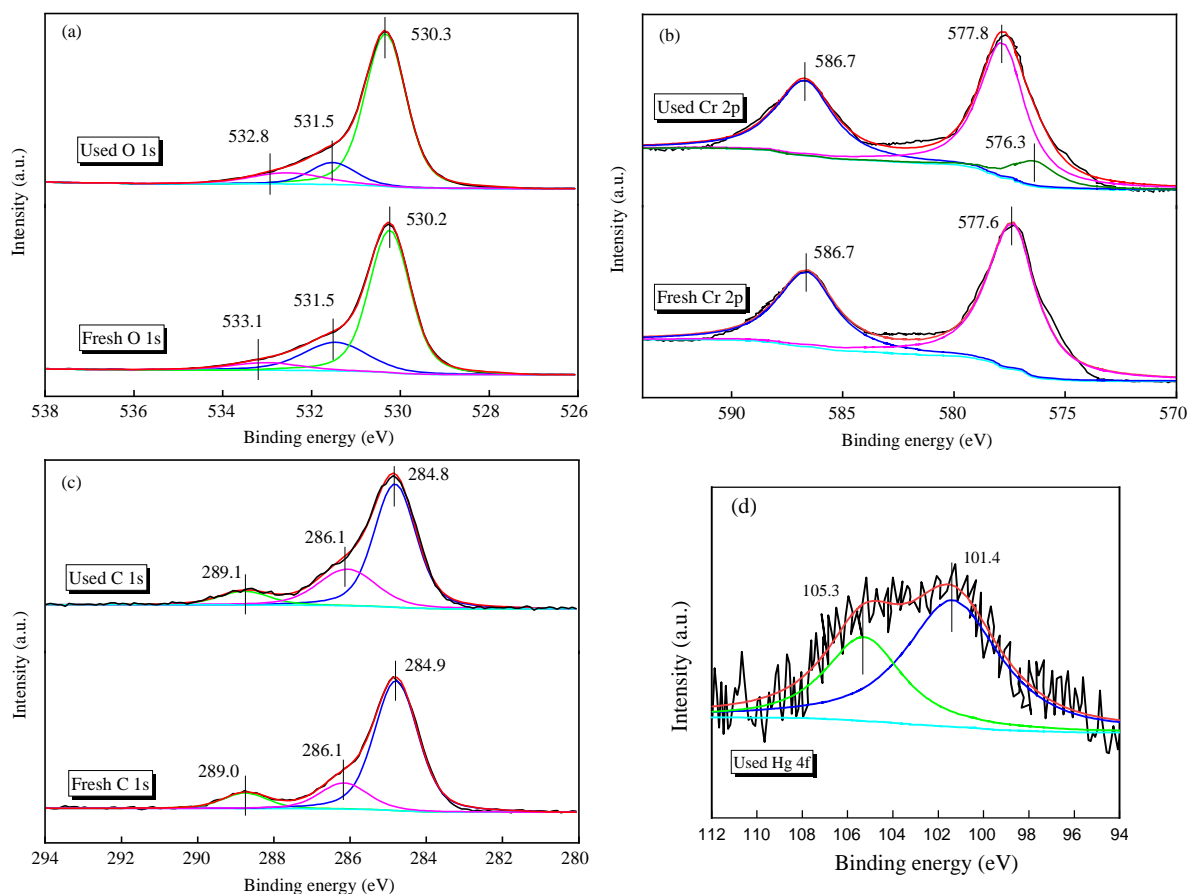


Fig. 16 XPS spectra of fresh and used MIL101-Cr sorbents for O 1s, Cr 2p, C 1s and Hg 4f.

(Reaction condition: $\text{N}_2+5\% \text{O}_2$, $203 \mu\text{g}/\text{m}^3$, $8 \times 10^5 \text{h}^{-1}$, $200 \text{ }^\circ\text{C}$)

Table 2 Surface compositions of the fresh and used sorbents based on XPS results.

	O 1s		C 1s	Cr 2p			Hg 4f	
	O^{2-}	O^*		Cr^{3+}	Cr^{2+}			
Binding energy (eV)	530.2	531.5	284.9	577.6	586.7	101.4	105.3	
Atomic concentration (%) (fresh)	70.2	23.4	70.4	61.9	38.1	0		
Atomic concentration (%) (used)	77.5	10.3	67.8	55.8	37.9	6.3	34.9	

Fig. 16 (d) shows the XPS spectra of Hg 4f for the spent MIL101-Cr sorbent. Two peaks corresponding to Hg^{2+} at 101.4 eV and 105.3 eV were observed, which indicate that Hg^0 is oxidized over the MIL101-Cr sorbent and remained on the surface of sorbent. However, Hg^0 could not be

detected on the surface of the used sorbent, which may be due to the escape of Hg^0 from the sample when pretreated under a vacuum before the XPS analysis.

3.3.3 Adsorption kinetics analysis

Several kinetic models, such as pseudo-first-order model, intra-particle diffusion equation, pseudo-second-order model and Elovich kinetic equation, had been used to determine the mechanism of the mercury adsorption process^{58, 59}. The pseudo-second-order model based on the Langmuir-type rate expression has been commonly used to describe the Hg^0 chemisorption process⁵⁷, from which the equilibrium adsorption capacity could be calculated as well.

From this study it has already concluded that the Hg^0 removal process over the MIL101-Cr sorbent at 200 °C belongs to chemisorption. Hence, the pseudo-second-order model was used to simulate the adsorption of Hg^0 by the MIL101-Cr sample as described by the following Eq. 21⁶⁰:

$$\frac{dq}{dt} = k_2 (q_e - q)^2 \quad (21)$$

With the boundary conditions $t=0$ to $t=t$ and $q=0$ to $q=q_t$, the above equation can be integrated as follows (Eqs. 22-23):

$$\frac{t}{q_t} = \frac{1}{k_2 q_e^2} + \frac{1}{q_e} t \quad (22)$$

$$q_t = \frac{t}{(1/k_2 q_e^2) + (t/q_e)} \quad (23)$$

Where q_t and q_e represent the amount of Hg^0 ($\mu\text{g/g}$) adsorbed at time t and equilibrium, respectively. k_2 represents the adsorption reaction rate constant of the pseudo-second-order sorption ($\text{g}/(\mu\text{g} \cdot \text{min})$). The values of k_2 and q_e could be obtained by fitting the Hg^0 adsorption curve. The accumulative Hg^0 adsorption capacity and model fitting results of MIL101-Cr at different temperatures are shown in Fig. 17. The correspond kinetic parameters (q_e , k_2) and correlation coefficient (R^2) for the MIL101-Cr

sorbent at different temperatures are listed in Table 3. The results indicate that the correlation coefficient (R^2) for the MIL101-Cr sorbent were greater than 0.999 at different adsorption temperatures. As it can be observed in Fig. 17, the pseudo-second-order model could fit the experimental data very well. This demonstrates that the pseudo-second-order model could be used to well describe the Hg^0 adsorption on the MIL101-Cr sorbent. The equilibrium adsorption capacity calculated for the sorbent amounted to 25656 $\mu g/g$ at 200 °C, which is much higher than those of the commercial activated carbon⁵⁷ and other sorbents investigated by previous studies^{38, 57, 59} (Table 1). Therefore, it can be concluded that the MIL101-Cr sorbent has great potential to be used as a promising Hg^0 removal sorbent.

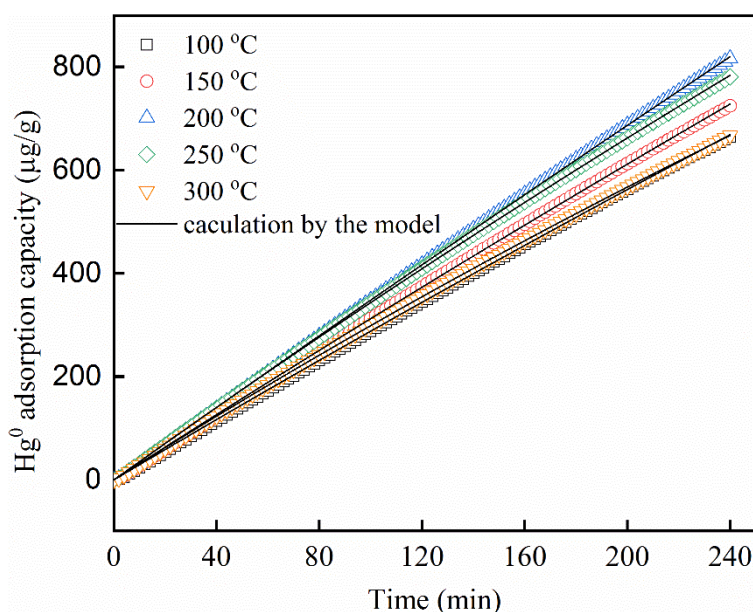


Fig. 17 Simulation of Hg^0 adsorption on MIL101-Cr by the pseudo-second-order model (Reaction condition: $N_2+5\% O_2$, $203 \mu g/m^3$, $8 \times 10^5 h^{-1}$, 200 °C)

Table 3 The kinetic parameters of the pseudo-second-order model for the MIL101-Cr sorbent.

Temperature (°C)	100	150	200	250	300
q_e ($\mu g/g$)	11853	14811	25656	9398	5600
$k_2 \times 10^8$ ($g/(\mu g \cdot min)$)	2.1	1.5	0.54	4.0	10.1
R^2	0.99986	0.99992	0.99993	0.99994	0.99997

4 Conclusions

In this study, the MIL101-Cr sorbent was prepared and used to remove Hg^0 from the simulated coal-fired flue gas. The results showed that the MIL101-Cr sorbent achieved the Hg^0 removal efficiency excess of 85% within 4 h at 200 °C with the condition of a relatively high Hg^0 inlet concentration and high GHSV. Both the O_2 and NO in the flue gas enhanced the Hg^0 removal. The effects of SO_2 in the flue gas on the Hg^0 removal were more complicated. Without the presence of O_2 in the flue gas, the Hg^0 adsorption was significantly impaired by SO_2 , whereas a low concentration of SO_2 had a negative effect on the Hg^0 removal with the help of O_2 in the flue gas. However, a high SO_2 content in the flue gas still significantly weakened the Hg^0 removal ability even in the presence of O_2 . The introduction of O_2 and NO to the flue gas could counteract the adverse effect of SO_2 on Hg^0 adsorption. H_2O slightly inhibited Hg^0 removal performance due to the competitive adsorptions between H_2O and Hg^0 . The XPS analysis indicated that the surface Cr^{3+} , oxygen species and $\text{C}=\text{O}$ groups on the surface of the MIL101-Cr sample acted as active adsorption/oxidation sites for Hg^0 . The Hg^0 removal by the MIL101-Cr sorbent belonged to chemisorption and could be described by pseudo-second-order model. The equilibrium adsorption capacity calculated for the sorbent amounted to $25656 \mu\text{g}\cdot\text{g}^{-1}$ at 200 °C. From the analysis of the experimental results of this study, it can be concluded that the MIL101-Cr sorbent has great potential to be used as a promising Hg^0 removal sorbent.

Acknowledgements

This project was financially supported by the National Key R&D Program of China (2018YFC1901200, 2016YFB0600604), the National Natural Science Foundation of China (51676040), the Jiangsu Basic Research Program (BK20181281), the Scientific Research Foundation

of Graduate School of Southeast University (3203009703), and the Postgraduate Research & Practice Innovation Program of Jiangsu Province (KYCX17_0079). We would also like to acknowledge the financial support from the China Scholarship Council (CSC) which enables the first author (Lu Dong) to complete the part of the reported work at the University of Nottingham under the supervision of the second corresponding author (Hao Liu).

References

- (1) Xu, W.; Li, T.; Hao, Q.; et al. Effect of Flue Gas Components on Hg⁰ Oxidation over Fe/HZSM-5 Catalyst. *Ind. Eng. Chem. Res.* 2015, 54, (1), 146-152.
- (2) Jampaiah, D.; Ippolito, S. J.; Sabri, Y. M.; et al. Ceria-zirconia modified MnOx catalysts for gaseous elemental mercury oxidation and adsorption. *Catal. Sci. Technol.* 2016, 6, 1792-1803.
- (3) Zhao, S.; Pudasainee, D.; Duan, Y.; et al. A review on mercury in coal combustion process: Content and occurrence forms in coal, transformation, sampling methods, emission and control technologies. *Prog. Energy Combust. Sci.* 2019, 73, 26-64.
- (4) Zhao, S.; Mei, J.; Xu, H.; et al. Research of mercury removal from sintering flue gas of iron and steel by the open metal site of Mil-101(Cr). *J. Hazard. Mater.* 2018, 351, 301-307.
- (5) Xu, Y.; Deng, F.; Pang, Q.; et al. Development of waste-derived sorbents from biomass and brominated flame retarded plastic for elemental mercury removal from coal-fired flue gas. *Chem. Eng. J.* 2018, 350, 911-919.
- (6) IEA's Coal Report 2018. <https://www.iea.org/coal2018/>
- (7) Zheng, J.; Shah, K. J.; Zhou, J.; et al. Impact of HCl and O₂ on removal of elemental mercury by heat-treated activated carbon: Integrated X-ray analysis. *Fuel Process. Technol.* 2017, 167, 11-17.

(8) Yang, Y.; Huang, Q.; Wang, Q.. Ignoring Emissions of Hg from Coal Ash and Desulfurized Gypsum Will Lead to Ineffective Mercury Control in Coal-Fired Power Plants in China. *Environ. Sci. Technol.* 2012, 46, (6), 3058-3059.

(9) Zhang, W.; Zhen, G.; Chen, L.; et al. Economic evaluation of health benefits of mercury emission controls for China and the neighboring countries in East Asia. *Energy Policy* 2017, 106, 579-587.

(10) Yang, W.; Liu, Z.; Xu, W.; et al. Removal of elemental mercury from flue gas using sargassum chars modified by NH₄Br reagent. *Fuel* 2018, 214, 196-206.

(11) Yang, J.; Ma, S.; Zhao, Y.; et al. Elemental Mercury Removal from Flue Gas over TiO₂ Catalyst in an Internal-Illuminated Honeycomb Photoreactor. *Ind. Eng. Chem. Res.* 2018, 57, (51), 17348-17355.

(12) Zhao, Y.; Yang, J.; Ma, S.; et al. Emission controls of mercury and other trace elements during coal combustion in China: a review. *Int. Geol. Rev.* 2018, 60, (5-6), 638-670.

(13) Sjostrom, S.; Durham, M.; Bustard, C. J.; et al. Activated carbon injection for mercury control: Overview. *Fuel* 2010, 89, (6), 1320-1322.

(14) Hsi, H.-C.; Tsai, C.-Y.; Kuo, T.-H.; et al. Development of low-concentration mercury adsorbents from biohydrogen-generation agricultural residues using sulfur impregnation. *Bioresour. Technol.* 2011, 102, (16), 7470-7477.

- (15) Zhao, B.; Yi, H.; Tang, X.; et al. Copper modified activated coke for mercury removal from coal-fired flue gas. *Chem. Eng. J. Chem. Eng. J.* 2016, 286, 585-593.
- (16) Zhao, H.; Fan, H.; Yang, G.; et al. Integrated Dynamic and Steady State Method and Its Application on the Screening of MoS₂ Nanosheet-Containing Adsorbents for Hg⁰ Capture. *Energy Fuels* 2018, 32, (4), 5338-5344.
- (17) Liu, H.; Zhao, Y.; Zhou, Y.; et al. Removal of gaseous elemental mercury by modified diatomite. *Sci. Total Environ.* 2019, 652, 651-659.
- (18) Li, H.; Zhu, W.; Yang, J.; et al. Sulfur abundant S/FeS₂ for efficient removal of mercury from coal-fired power plants. *Fuel* 2018, 232, 476-484.
- (19) Li, H.; Zhu, L.; Wu, S.; et al. Synergy of CuO and CeO₂ combination for mercury oxidation under low-temperature selective catalytic reduction atmosphere. *Int. J. Coal Geol.* 2017, 170, 69-76.
- (20) Yang, J.; Zhao, Y.; Zhang, S.; et al. Mercury removal from flue gas by magnetospheres present in fly ash: Role of iron species and modification by HF. *Fuel Process. Technol.* 2017, 167, 263-270.
- (21) Yang, J.; Zhao, Y.; Zhang, J.; et al. Regenerable Cobalt Oxide Loaded Magnetosphere Catalyst from Fly Ash for Mercury Removal in Coal Combustion Flue Gas. *Environ. Sci. Technol.* 2014, 48, (24), 14837-14843.

(22) Yang, J.; Zhu, W.; et al. Selenium Functionalized Metal–Organic Framework MIL-101 for Efficient and Permanent Sequestration of Mercury. *Environ. Sci. Technol.* 2019, 53, (4), 2260-2268.

(23) Zhang, W.; Yan, Z.; Gao, J.; et al. Metal–organic framework UiO-66 modified magnetite@silica core–shell magnetic microspheres for magnetic solid-phase extraction of domoic acid from shellfish samples. *J. Chromatogr. A* 2015, 1400, 10-18.

(24) Yang, Y.; Ma, X.; Feng, F.; et al. Magnetic solid-phase extraction of triclosan using core-shell Fe₃O₄@MIL-100 magnetic nanoparticles, and its determination by HPLC with UV detection. *Microchim. Acta* 2016, 183, (8), 2467-2472.

(25) Shi, Z.; Xu, C.; Guan, H.; et al. Magnetic metal organic frameworks (MOFs) composite for removal of lead and malachite green in wastewater. *Colloids Surf., A* 2018, 539, 382-390.

(26) Sun, X.; Gao, G.; Yan, D.; et al. Synthesis and electrochemical properties of Fe₃O₄@MOF core-shell microspheres as an anode for lithium ion battery application. *Appl. Surf. Sci.* 2017, 405, 52-59.

(27) Qasem, N. A. A.; Ben-Mansour, R.; Habib, M. A.. An efficient CO₂ adsorptive storage using MOF-5 and MOF-177. *Appl. Energy* 2018, 210, 317-326.

(28) Zhang, X.; Shen, B.; Zhu, S.; et al. UiO-66 and its Br-modified derivatives for elemental mercury removal. *J. Hazard. Mater.* 2016, 320, 556-563.

- (29) Chen, D.; Zhao, S.; Qu, Z.; et al. Cu-BTC as a novel material for elemental mercury removal from sintering gas. *Fuel* 2018, 217, 297-305.
- (30) Zhang, X.; Shen, B.; Shen, F.; et al. The behavior of the manganese-cerium loaded metal-organic framework in elemental mercury and NO removal from flue gas. *Chem. Eng. J.* 2017, 326, 551-560.
- (31) Granite, E. J.; Pennline, H. W.; Hargis, R. A.. Novel Sorbents for Mercury Removal from Flue Gas. *Ind. Eng. Chem. Res.* 2000, 39, (4), 1020-1029.
- (32) Chen, G.; Zhang, D.; Zhang, A.; et al. CrO_x-MnO_x-TiO₂ adsorbent with high resistance to SO₂ poisoning for Hg⁰ removal at low temperature. *J. Ind. Eng. Chem.* 2017, 55, 119-127.
- (33) Wang, S.; Zhang, Q.; Zhang, G.; et al. Effects of sintering flue gas properties on simultaneous removal of SO₂ and NO by ammonia-Fe(II)EDTA absorption. *J. Energy Inst.* 2017, 90, (4), 522-527.
- (34) Yan, N.; Chen, W.; Chen, J.; et al. Significance of RuO₂ Modified SCR Catalyst for Elemental Mercury Oxidation in Coal-fired Flue Gas. *Environ. Sci. Technol.* 2011, 45, (13), 5725-5730.
- (35) Bromberg, L.; Diao, Y.; Wu, H.; et al. Chromium(III) Terephthalate Metal Organic Framework (MIL-101): HF-Free Synthesis, Structure, Polyoxometalate Composites, and Catalytic Properties. *Chem. Mater.* 2012, 24, (9), 1664-1675.

(36) Yang, C.; Yan, X.. Metal–Organic Framework MIL-101(Cr) for High-Performance Liquid Chromatographic Separation of Substituted Aromatics. *Anal. Chem.* 2011, 83, (18), 7144-7150.

(37) Wang, T.; Wu, J.; Zhang, Y.; et al. Increasing the chlorine active sites in the micropores of biochar for improved mercury adsorption. *Fuel* 2018, 229, 60-67.

(38) Cai, J.; Shen, B.; Li, Z.; et al. Removal of elemental mercury by clays impregnated with KI and KBr. *Chem. Eng. J.* 2014, 241, 19-27.

(39) Yang, J.; Zhao, Y.; Liang, S.; et al. Magnetic iron–manganese binary oxide supported on carbon nanofiber (Fe_{3-x}Mn_xO₄/CNF) for efficient removal of Hg⁰ from coal combustion flue gas. *Chem. Eng. J.* 2018, 334, 216-224.

(40) Tan, Z.; Su, S.; Qiu, J.; et al. Preparation and characterization of Fe₂O₃–SiO₂ composite and its effect on elemental mercury removal. *Chem. Eng. J.* 2012, 195-196, 218-225.

(41) Dong, L.; Xie, J.; Fan, G.; et al. Experimental and theoretical analysis of elemental mercury adsorption on Fe₃O₄/Ag composites. *Korean J. Chem. Eng.* 2017, 34, (11), 2861-2869.

(42) Li, H.; Wu, C.; Li, Y.; et al. Superior activity of MnO_x-CeO₂/TiO₂ catalyst for catalytic oxidation of elemental mercury at low flue gas temperatures. *Appl. Catal., B* 2012, 111-112, 381-388.

(43) Yang, W.; Liu, Y.; Wang, Q.; et al. Removal of elemental mercury from flue gas using wheat straw chars modified by Mn-Ce mixed oxides with ultrasonic-assisted impregnation. *Chem. Eng. J.* 2017, 326, 169-181.

(44) Xu, W.; Adewuyi, Y. G.; Liu, Y.; et al. Removal of elemental mercury from flue gas using CuOx and CeO₂ modified rice straw chars enhanced by ultrasound. *Fuel Process. Technol.* 2018, 170, 21-31.

(45) Li, Y.; Murphy, P. D.; Wu, C.; et al. Development of Silica/Vanadia/Titania Catalysts for Removal of Elemental Mercury from Coal-Combustion Flue Gas. *Environ. Sci. Technol.* 2008, 42, (14), 5304-5309.

(46) Yang, J.; Zhu, W.; Zhang, S.; et al. Role of flue gas components in Hg⁰ oxidation over La_{0.8}Ce_{0.2}MnO₃ perovskite catalyst in coal combustion flue gas. *Chem. Eng. J.* 2019, 360, 1656-1666.

(47) Wu, H.; Li, C.; Zhao, L.; et al. Removal of Gaseous Elemental Mercury by Cylindrical Activated Coke Loaded with CoOx-CeO₂ from Simulated Coal Combustion Flue Gas. *Energy Fuels* 2015, 29, (10), 6747-6757.

(48) Li, Y.; Murphy, P.; Wu, C.. Removal of elemental mercury from simulated coal-combustion flue gas using a SiO₂-TiO₂ nanocomposite. *Fuel Process. Technol.* 2008, 89, (6), 567-573.

(49) Xie, Y.; Li, C.; Zhao, L.; et al. Experimental study on Hg⁰ removal from flue gas over columnar MnOx-CeO₂/activated coke. *Appl. Surf. Sci.* 2015, 333, 59-67.

(50) Pang, L.; Yang, P.; Yang, H.; et al. Application of Fe₃O₄@MIL-100 (Fe) core-shell magnetic microspheres for evaluating the sorption of organophosphate esters to dissolved organic matter (DOM). *Sci. Total Environ.* 2018, 626, 42-47.

(51) Tang, Q., X.; Zhang, Y.; Zhong, Wei.; et al. Fe₃O₄ and metal-organic framework MIL-101(Fe) composites catalyze luminol chemiluminescence for sensitively sensing hydrogen peroxide and glucose. *Talanta* 2018, 179, 43-50.

(52) Yang, J.; Zhao, Y.; Ma, S.; et al. Mercury Removal by Magnetic Biochar Derived from Simultaneous Activation and Magnetization of Sawdust. *Environ. Sci. Technol.* 2016, 50, (21), 12040-12047.

(53) Xu, Y.; Luo, G.; Pang, Q.; et al. Adsorption and catalytic oxidation of elemental mercury over regenerable magnetic Fe-Ce mixed oxides modified by non-thermal plasma treatment. *Chem. Eng. J.* 2019, 358, 1454-1463.

(54) Zhang, C.; Song, W.; Zhang, X.; et al. Synthesis and evaluation of activated carbon spheres with copper modification for gaseous elemental mercury removal. *J. Porous Mater.* 2018.

(55) Shen, B.; Tian, L.; Li, F.; et al. Elemental mercury removal by the modified biochar from waste tea. *Fuel* 2017, 187, 189-196.

(56) Li, X.; Cao, J.; Zhang, W.. Stoichiometry of Cr(VI) Immobilization Using Nanoscale Zerovalent Iron (nZVI): A Study with High-Resolution X-Ray Photoelectron Spectroscopy (HR-XPS). *Ind. Eng. Chem. Res.* 2008, 47, (7), 2131-2139.

(57) Xu, Y.; Luo, G.; He, S.; et al. Efficient removal of elemental mercury by magnetic chlorinated biochars derived from co-pyrolysis of Fe(NO₃)₃-laden wood and polyvinyl chloride waste. *Fuel* 2019, 239, 982-990.

(58) Skodras, G.; Diamantopoulou, I.; Pantoleontos, G.; et al. Kinetic studies of elemental mercury adsorption in activated carbon fixed bed reactor. *J. Hazard. Mater.* 2008, 158, (1), 1-13.

(59) Li, G.; Wang, S.; Wu, Q.; et al. Mechanism identification of temperature influence on mercury adsorption capacity of different halides modified bio-chars. *Chem. Eng. J.* 2017, 315, 251-261.

(60) Cáceres, L.; Escudey, M.; Fuentes, E.; et al. Modeling the sorption kinetic of metsulfuron-methyl on Andisols and Ultisols volcanic ash-derived soils: Kinetics parameters and solute transport mechanisms. *J. Hazard. Mater.* 2010, 179, (1), 795-803.